



Original Article

Geochemistry and geochronology of Carboniferous volcanic rocks from the Edren range, Trans-Altai Zone, SW Mongolia

Otgonkhoo Javkhlan^{*1,2,4} , Anaad Chimedtseren^{2,5} , Ochir Gerel² ,
Bayaraa Batkhishig^{2,3} , Baatar Munkhtsengel^{2,3} 

¹Telmen Resource LLC, TMK Energy Limited, Ulaanbaatar 13336, Mongolia

²Geoscience Center, Mongolian University of Science and Technology, Ulaanbaatar 14191, Mongolia

³School of Geology and Mining Engineering, Mongolian University of Science and Technology, Ulaanbaatar 14191, Mongolia

⁴Institute of Mineral Resources, Chinese Academy of Geological Sciences, Beijing 100037, China

⁵Mongolian Natural History Museum, Ulaanbaatar 15141, Mongolia

*Corresponding author: o.javkhlan@must.edu.mn, ORCID: [0000-0003-1681-348X](https://orcid.org/0000-0003-1681-348X)

ARTICLE INFO

Article history:

Received 02 November, 2022

Revised 01 December, 2022

Accepted 30 December, 2022

ABSTRACT

The Edren range of the Trans-Altai zone is situated in the central south part of the Central Asian Orogenic Belt. The Edren range is composed primarily of volcano-sedimentary rocks that were weakly metamorphosed during the Devonian to Carboniferous periods. These rocks were then intruded by granite plutons during the Carboniferous to Permian periods. The area is further divided into two units, the Edrengeen Nuruu and Davkhar Khar, which are separated by the Khyariingun thrust fault. Three episodes of magmatism have been recognized in the Edren range. The earliest episode of magmatism at c. 360 Ma is present in the Edrengeen Nuruu unit. A younger episode of magmatism at c. 330 Ma is present in the Davkhar Khar unit. The youngest episode of magmatism, dated at c. 300 Ma is represented by rhyolite porphyry dykes in the Edrengeen Nuruu unit. The first episode of c. 360 Ma volcanism, developed in a continental arc setting, produced relatively contaminated basalt-andesite magma ($\text{SiO}_2=49.39-57.65$ wt%; $\text{Mg}\#=27-47$; $(\text{La}/\text{Yb})_N=3.24-15.39$) with relatively low initial ϵNd -values (from ca. +1.9 to +4.3) by subduction of the oceanic crust, developed on Devonian continental juvenile crust. Following subduction, steady northward transition of volcanic arc occurred. At c. 330 Ma continuous subduction of oceanic crust produced basalt-andesite-rhyolite magma ($\text{SiO}_2=47.16-72.76$ wt%; $\text{Mg}\#=4-48$; $(\text{La}/\text{Yb})_N=1.34-10.91$) with higher initial ϵNd -values (from ca. +1.6 to +5.8). At c. 300 Ma, rhyolite porphyry dykes ($\text{SiO}_2=75.70-75.86$ wt%; $\text{Mg}\#=5-6$; $\epsilon\text{Nd}=+2.6$) developed in the Edrengeen Nuruu unit by subduction or collision-related magmatism.

Keywords: Edrengeen Nuruu, Dulaan Khar, U-Pb age, magmatism

INTRODUCTION

The Trans-Altai Zone is an oceanic domain consisting of Ordovician to Devonian ophiolites together with Silurian to Devonian-Carboniferous oceanic sediments and volcanic rocks (Guy et al., 2014; Jian et al., 2014; Kröner et al., 2010; Ruzhentsev and Pospelov, 1992,

Ruzhentsev, 2001). This zone is situated in the south part of the Mongol Altai Range among the branch ranges of Edren, Sumankhad, Ajbogd, Dund, and Khuviinkhar; separated by the Trans-Altai fault from the Gobi-Altai Zone to the north, and by the Gobi Tian Shan fault from the Gobi Tian Shan Zone to the south (Fig. 1b)

(Kröner et al., 2010). The Trans-Altai zone is situated in the central south part of the Central Asian Orogenic Belt (CAOB). The CAOB or Altaids, is one of the largest accretionary orogens on Earth (Jahn et al., 2004; Safanova et al., 2011; Sengör and Natal'In, 1996; Windley et al., 2007) developed between the Siberian craton in the north, the Tarim craton in the south-west, and the North China craton in the south (Jahn et al., 2000) (Fig. 1a). Tectonic evolution of the CAOB recently suggests that Neoproterozoic to Carboniferous accretionary continental growth, followed by Permian to Triassic collisional deformation (Lehmann et al., 2010; Schulmann and Paterson, 2011; Xiao et al., 2015, 2018). The accretionary continental growth is associated with formation of giant magmatic arcs (e.g., Jahn, 2004) which are progressively migrated to Tarim and North China craton due to a slab retreat (Jahn, 2010). Newly formed juvenile crust assembled by previous giant magmatic arcs or old continental crust were recycled during a major period of collisional deformation (Guy et al., 2014; Kozlovsky et al., 2015; Kröner et al., 2014). Previous works of Hanžl et al. (2008), Yarmolyuk et al. (2008) and Nguyen et al. (2018) who described intrusive and volcanic rocks in the wider area of the Trans-Altai Zone and latter correlate closely with the Dulate-Yemaquan arc system in eastern Junggar (Nguyen et al., 2018; Xiao and Kusky, 2009). In this study, we focus on more narrow area of eastern part of the Trans-Altai Zone in the Khyariingun Khudag area (Fig. 1b) of the Edren range, in order to understand a slab retreating process in detail. Previous studies suggested formation of an Early Carboniferous volcanic arc (Nguyen et al., 2018), with a Late Carboniferous bimodal volcanic suite related to a back-arc extensional environment (Zhu et al., 2017). However, little detailed geochemical and geochronological work was done on the Edren range. Here, we present new geochemical and geochronological data on volcanic and plutonic rocks. Results of the study suggest that the magmatism of the Edren range developed because of multiple events of oceanic subduction and slab retreat observed during the Early Carboniferous.

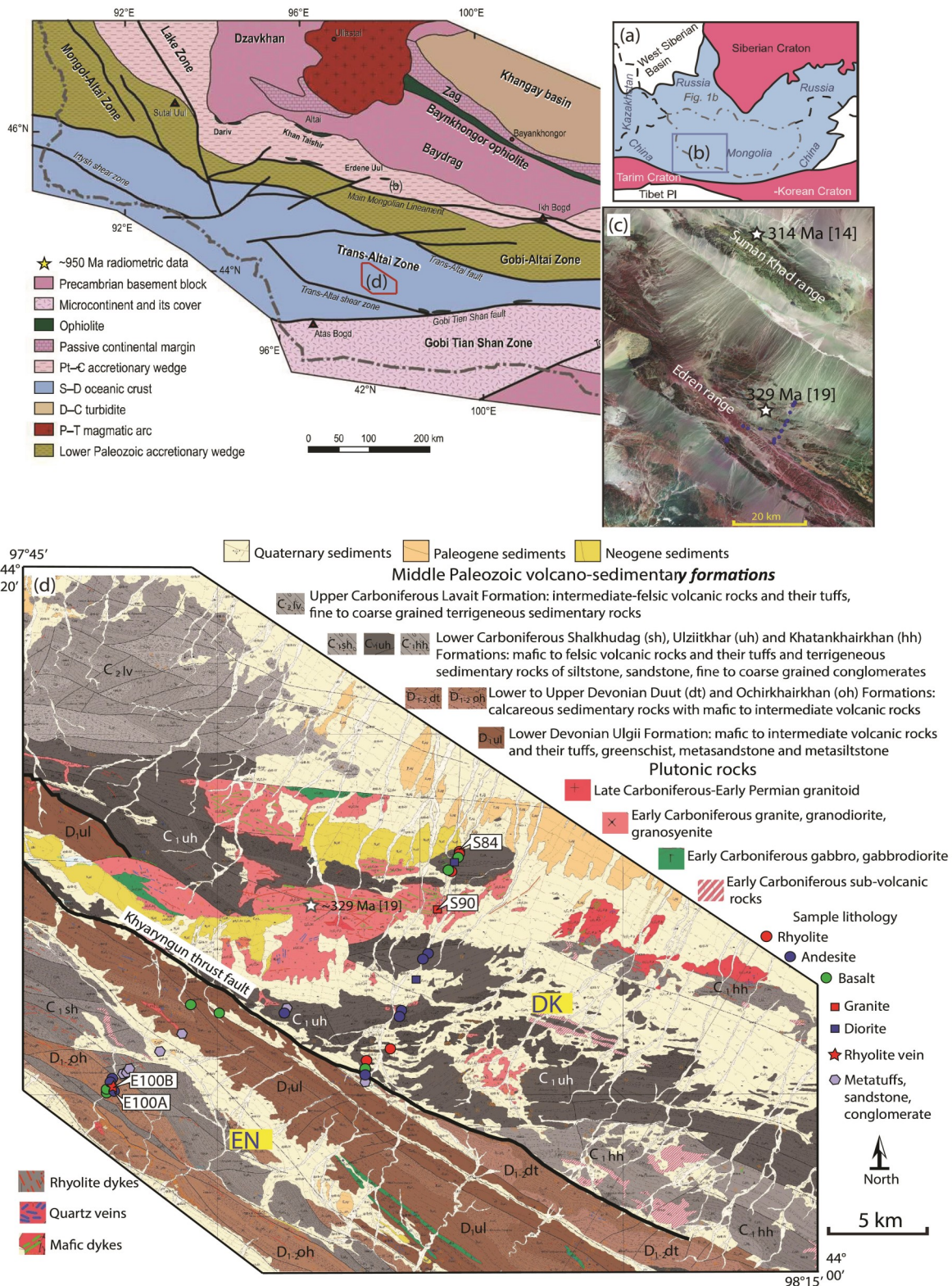
GEOLOGICAL BACKGROUND

The Trans-Altai Zone is subdivided into the Khuvynkhar, Edren, Baaran, Zuulun and Baitag terranes (Badarch et al., 2002). Our study area is within the Edren terrane. The Edren terrane includes Devonian to Carboniferous volcano-sedimentary rocks containing limestone lenses with Early Devonian brachiopods (Šourek et al., 2003). The terrane is intruded by Carboniferous to Permian granite plutons. The rocks have undergone intense brittle-ductile deformation associated with greenschist-facies metamorphism (Nguyen et al., 2018).

In the Khyariingun Khudag area, we conducted field observation of the section through Devonian sedimentary sequences and thick Carboniferous volcanic sequence intruded by granitoid (Fig. 1d). The study area can be divided into two units, Edreniingun Nuruu (EN) and Davkhar Khar (DK) by the Khyariingun thrust fault (Fig. 1d) (Togtokh et al., 2020).

The EN unit extends to NW, covering the southern half of the Edren range (Fig. 1d). Stratigraphically, the lower part of the EN unit is composed mainly of interleaved layers of Lower to Middle Devonian fauna-bearing sedimentary sequences of sandstone, siltstone, and limestone, layers of metabasalts, volcanic pyroclasts and gabbroid sill-like bodies. Locally, volcanic pyroclastics contain clasts of serpentinite (Gordienko, 1987). Lower-Middle Devonian corals, brachiopods, and crinoids are found in the EN unit (Togtokh et al., 2020). The upper part of the EN unit is represented by the volcano-terrigenous formation containing Mississippian aged faunas of brachiopods, crinoids, bivalvia and flora. Volcanic rocks of this formation mainly consist of andesite, dacite, basalts and their tuffs (Figs. 2a, c and d). Both Devonian and Carboniferous sequences are crosscut by thick (<10 m width) rhyolite dykes (Figs. 2c and d) (Togtokh et al., 2020).

The DK unit extends to NW, covering the northern half of the Edren range (Fig. 1d). Stratigraphically, Upper Silurian bodies of peridotite and gabbro occur in the lowest part of a section. These are covered by a Lower-Middle Devonian coral and brachiopod-bearing terrigenous-carbonatic-volcanic formation, an oceanic reef (Togtokh et al., 2020). Upward to



the section, an Upper Devonian-Lower Carboniferous brachiopod-bearing terrigenous fore-arc formation is covered by the Lower Carboniferous terrigenous-volcanic formation. The lower member of the terrigenous sedimentary rocks contains Tournaisian crinoid and ostracod faunas. The upper member of volcanic rocks is composed of basalt, andesite and rhyolite (Fig. 2b). The Lower Carboniferous terrigenous-volcanic formation is intruded by the Bayan-Airag plutonic complex consisting of gabbro, monzonite and granite as well as Late Carboniferous-Lower Permian granitoid (Togtokh et al., 2020). Yarmolyuk et al. (2008) reported U-Pb zircon ages on biotite-hornblende quartz diorite from Bayan-Airag complex as 329 ± 1 Ma).

Most of the volcanic rocks from the EN and DK units were deformed and altered by greenschist facies metamorphism. NW-SE directed foliation planes dipping to the SW are developed in the volcanic and sedimentary sequences. Apart from the foliation planes, bedding planes dipping

from NE to SW are also observed in some of the outcrops of the sedimentary sequences (Munkhtsengel et al., 2018).

Petrography

Sixteen volcanic (mafic to felsic) rock samples, and two rhyolite porphyry dyke samples were collected along the field section from the EN and DK units (Fig. 1d). Basaltic rocks from the EN unit have a porphyritic texture, with fine-grained plagioclase, pyroxene and secondary hornblende, chlorite, epidote in the matrix and large plagioclase phenocrysts (up to 5 mm) with sieve texture (Fig. 3a). Plagioclase is commonly altered to secondary sericite, epidote and carbonaceous material. Andesite from the EN unit has an intersertal texture with fine-grained altered microlithic groundmass composed of plagioclase, secondary chlorite, amphibole and calcite (Fig. 3b). Plagioclase is commonly partially replaced by fine-grained epidote and sericite. The groundmass is overprinted by subhedral to euhedral secondary amphibole with

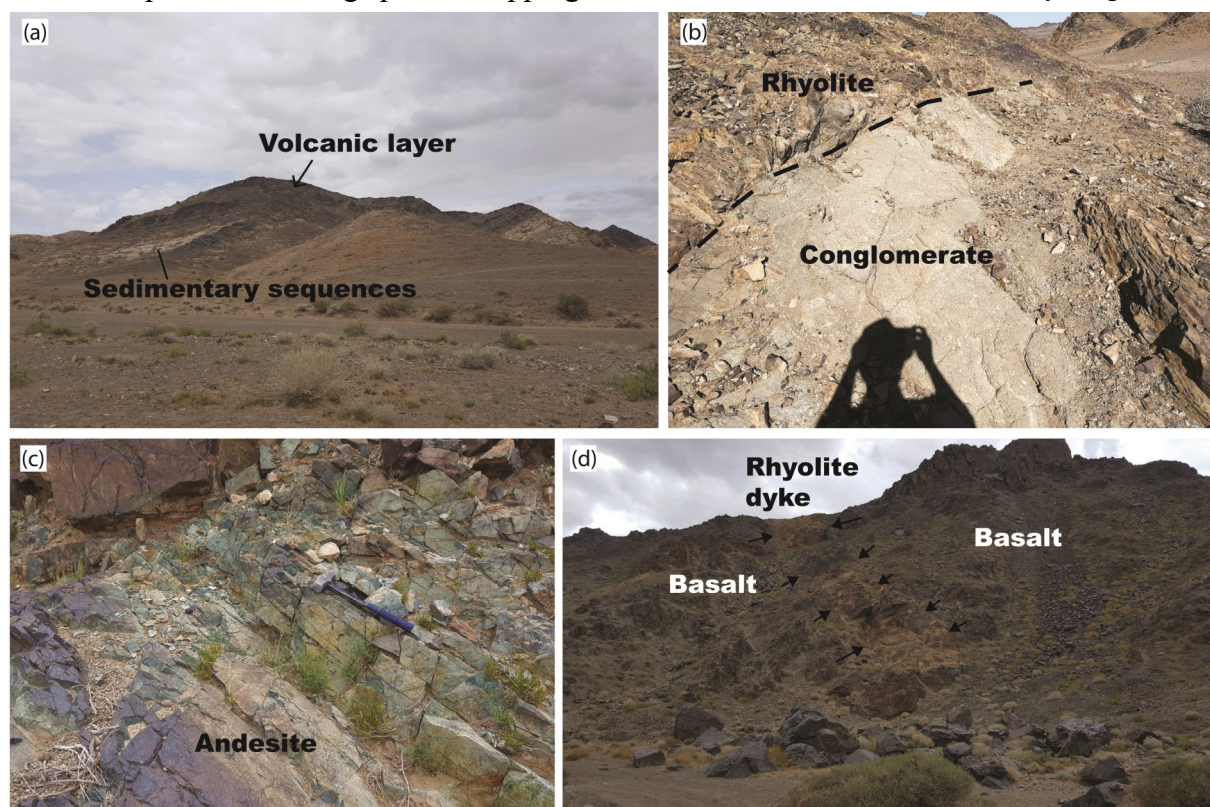


Fig. 2. Field photos of the Edren range (a) A volcanic layer laying on the sedimentary unit in the EN unit; (b) Boundary zone between EN and DK units. A terrigenous formation (conglomerate and sandstone) thrust over (dashed line) a rhyolite layer of the DK unit; (c) An andesite layer in the EN unit; (d) A basalt layer cross-cut by rhyolite dyke in the EN unit.

chlorite and Fe-Ti oxide. The rhyolite dykes developed in the EN unit consist mainly of K-feldspar, quartz, plagioclase, minor amounts of sericite, epidote and calcite. Magnetite and zircon occur as accessory minerals. The tabular phenocrysts of potassium feldspar are up to 1 cm in size, mostly altered to sericite and calcite. The subhedral plagioclase has a prismatic shape, and some phenocrysts have a pseudomorphic structure, due to epidote-calcite alteration. The main matrix of the rhyolite dyke consists mainly of fine-grained quartz and feldspar.

The basaltic rocks from the DK unit have a porphyritic texture, with fine-grained plagioclase, pyroxene and secondary hornblende in the intergranular matrix and large clinopyroxene, plagioclase and secondary amphibole phenocrysts (up to 2 mm) (Fig. 3d). Plagioclase is commonly altered to secondary sericite and epidote in the core part, whereas clinopyroxene is commonly overprinted by green hornblende. The andesites and trachyandesite from the DK unit have a porphyritic texture with fine-grained altered

groundmass (Fig. 3e). The fine-grained groundmass is made of altered plagioclase, hornblende, and chlorite. Plagioclase is the main mineral, occurring as large laths or tabular phenocrysts (up to 1 mm long). It is commonly replaced by fine-grained epidote and sericite. Poikilitic textured altered phenocrysts of K-feldspar within the matrix occur as euhedral or subhedral crystals, up to 3 mm long. They contain euhedral hornblende and plagioclase as inclusions. Subhedral to euhedral amphibole mainly occurs in the groundmass and some is replaced by chlorite and Fe-Ti oxide.

The dacite-rhyolite from the DK unit has K-feldspar and quartz phenocrysts (Fig. 3f). They are euhedral to subhedral in shape. Some of the poikilitic K-feldspar crystals are up to 3 mm long. Sodic plagioclase is prismatic and strongly replaced by sericite or epidote. The fine-grained groundmass is made of feldspar and quartz. Amphiboles are rare and overprinted by chlorite and Fe-Ti oxide. Fine-grained recrystallized quartz aggregates have a granular texture.

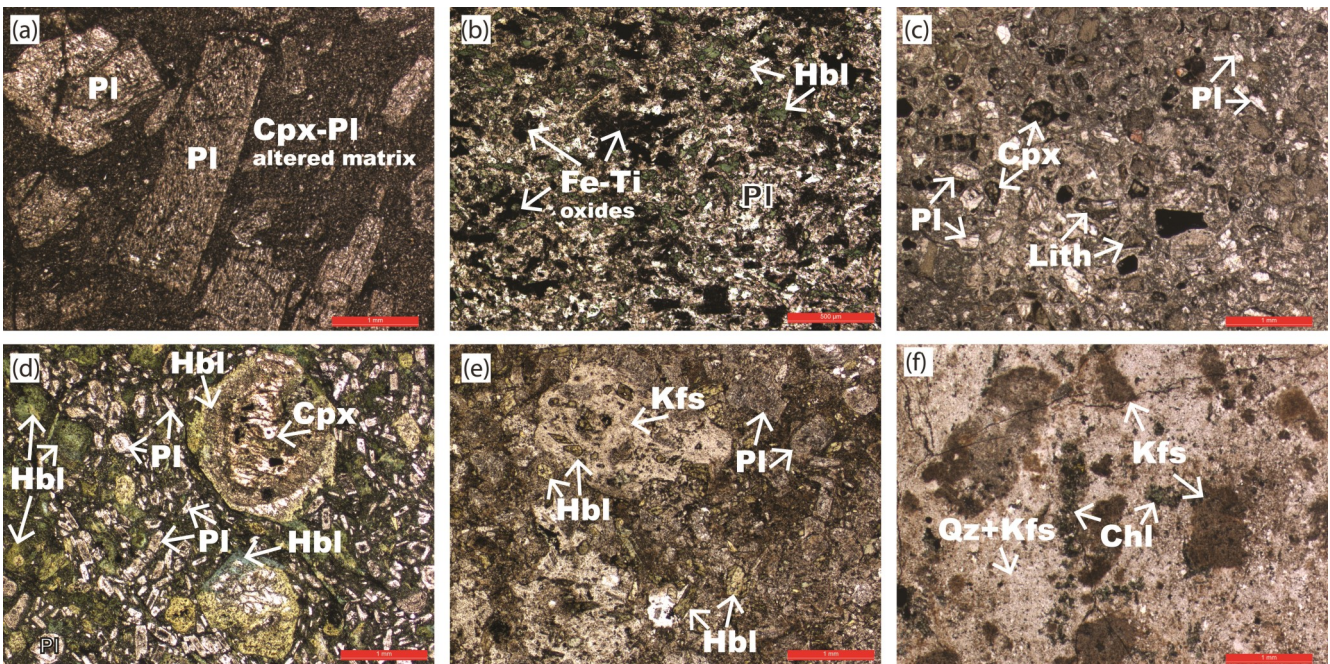


Fig. 3. (a) A porphyritic basalt from the EN unit with coarse-grained altered phenocrysts and altered groundmass; (b) Andesite from the EN unit displaying an intersertal texture with a fine-grained altered microlithic groundmass; (c) A -basaltic tuff from the EN unit with rounded grains of feldspars, pyroxene and lithic materials; (d) An altered porphyritic basalt from the DK unit with fine-grained plagioclase, pyroxene and secondary hornblende in the intergranular matrix and large phenocrysts of clinopyroxene partially overprinted by hornblende and plagioclase; (e) An andesite from the DK unit displaying porphyritic texture with a fine-grained altered groundmass; (f) A rhyolite from the DK unit with K-feldspar and quartz phenocrysts.

ANALYTICAL METHODS

Zircon U-Pb dating

Four least-altered samples, representing felsic to intermediate volcanic and granitoid rocks, were selected for LA-ICP-MS U-Pb zircon geochronology to determine the ages in the Edren range. They were collected from rhyolite (sample S84) from the Ulziitkhar Formation, andesite (sample E100A) and rhyolite dyke (sample E100B) from the Shalkhudag Formation and granite (sample S90) from the Bayan-Airag complex (Fig. 1d).

The analyzed zircons were separated from the samples using the following techniques that included crushing, pulverizing, the use of a Wilfley Table, heavy liquid, magnetic separation, and handpicking. The zircons were then mounted in epoxy and polished. Reflected and transmitted light photomicrographs, and cathodoluminescence (CL) images were used to determine the internal textures of the sectioned zircon grains to target areas within the least-fractured and inclusion-free zones.

All U-Pb isotope data were collected at the Institute of Mineral Resources of the Chinese Academy of Geological Sciences in Beijing using a multi-collector inductively coupled plasma mass spectrometer (LA-MC-ICP-MS) using a Thermo Finnigan Neptune MC-ICP-MS coupled to a New Wave 213 Nd-YAG laser ablation system. The spot size is ~30 μm . Hou et al. (2009) describe the operating conditions for the laser ablation system and the MC-ICP-MS instrument and data reduction.

The array of four multi-ion-counters and three faraday cups allow for simultaneous detection of ^{202}Hg (on IC5), ^{204}Hg , ^{204}Pb (on IC4), ^{206}Pb (on IC3), ^{207}Pb (on IC2), ^{208}Pb (on L4), ^{232}Th (on H2), and ^{238}U (on H4) ion signals. The make-up gas included argon and helium (the carrier gas) mixed via a T-connector before entering the ICP. Each analysis incorporated a background acquisition of approximately 20-30 s (gas blank) followed by a 30 s data acquisition from the sample. Off-line raw data selection, integration of background and analytic signals, and time-drift correction and quantitative calibration for U-Pb dating was performed using the ICPMS Data Cal software (Liu et al., 2010). The standard GJ1 zircon was analyzed twice every 5

-10 analyses. Time-dependent drifts of the U-Th-Pb isotopic ratios were corrected using linear interpolation with time for every 5-10 analyses according to the variations in the GJ1 analyses, as outlined by Liu et al. (2010), with the preferred U-Th-Pb isotopic ratios outlined by Jackson et al. (2004). The uncertainty of preferred values for the external standard GJ1 was propagated to the ultimate results of the samples. The U, Th and Pb concentrations were calibrated against the M127 zircon standard containing 923 ppm U, 439 ppm Th, and the Th/U ratio of 0.48 (Nasdala et al., 2008). Concordia diagrams and weighted mean calculations were made using Isoplot/Ex_ver3 (Ludwig, 2003). The Plesovice standard zircon was dated as an unknown sample and yielded a weighted mean $^{206}\text{Pb}/^{238}\text{U}$ age of 337 ± 2 Ma (2σ , $n=12$), which is in good agreement with the recommended $^{206}\text{Pb}/^{238}\text{U}$ age of 337.13 ± 0.37 Ma (2σ) (Sláma et al., 2008). Uncertainties reported at 95% confidence level.

Major and trace element analysis

The Analytical Center of the Beijing Institute of Geology for Nuclear Industry (ACBIGNI) undertook the whole-rock analyses. Major element compositions were determined by X-ray fluorescence (PhilipPW2404) using fused disks. Trace elements were determined by ICP-MS (Finnigan-MAT Element I) after acid digestion of samples in Teflon bombs. Analytical precision and accuracy are better than 5% for major elements and 10% for trace elements.

Rb-Sr and Sm-Nd isotope analyses

Whole rock Rb-Sr and Sm-Nd isotopic ratios were determined by TIMS using an ISOPROBE-T (IsoProbe-TTM (IsotopX Ltd) | EVISA's Instruments Database (speciation.net)) at the ACBIGNI. The $^{147}\text{Sm}/^{144}\text{Nd}$ and $^{87}\text{Rb}/^{86}\text{Sr}$ ratios were calculated using Sm, Nd, Rb, and Sr concentrations measured with the ICP-MS. The measured $^{143}\text{Nd}/^{144}\text{Nd}$ and $^{87}\text{Sr}/^{86}\text{Sr}$ ratios were normalized to $^{146}\text{Nd}/^{144}\text{Nd}=0.7219$ and $^{86}\text{Sr}/^{88}\text{Sr}=0.1194$, respectively. The SHINESTU Nd standards, and NBS-987 Sr standards were measured during the course of analyses, yielding a $^{143}\text{Nd}/^{144}\text{Nd}$ ratio of 0.51212 ± 3 (2σ), and $^{87}\text{Sr}/^{86}\text{Sr}=0.71025\pm 7$ (2σ), respectively.

RESULT

Zircon U–Pb geochronology

Representative zircon CL images and a series of concordia diagrams with weighted mean $^{206}\text{Pb}/^{238}\text{U}$ ages for 4 samples from the Edren range are shown in Fig. 4. Analyzed spots with U-Pb ages are listed in [Supplementary table 1](#). Inherited zircons with older $^{206}\text{Pb}/^{238}\text{U}$ ages and zircons with a concordance of less than 90% excluded from the age calculations.

The andesite sample (E100A) from the Shalkhudag Formation in the EN unit has euhedral zircons that are from 56 μm to 96 μm long, with length-width ratios of approximately 1:1 to 3:1. Some of the zircons contain small inclusions. Most of the zircons display fine concentric oscillatory zoning patterns that are characteristic of a magmatic origin. Fourteen analyses of zircons have highly varied abundances of ^{232}Th (34-687 ppm) and ^{238}U (42-1434 ppm) with Th/U ratios ranging from 0.09 to 1.15. Six analyses are concordant with a weighted mean $^{206}\text{Pb}/^{238}\text{U}$ age of 359 ± 5 Ma

(MSWD=0.81) (Fig. 4b). The analyses are the same identical within error, recording magmatism between Lower Carboniferous and Upper Devonian. Four zircon grains yielded much higher $^{206}\text{Pb}/^{238}\text{U}$ ages of c. 748 Ma, 750 Ma, 625 Ma and 474 Ma, likely indicate inherited zircons from older crustal rocks.

Sample E100B from a rhyolite porphyry dyke that cuts across the andesite outcrop of Shalkhudag Formation in the EN unit was dated. The zircons from the rhyolite dyke occur as subhedral to euhedral crystal, which are 30 μm to 130 μm long, with length/width ratios of between 1:1 and 3:1. Most of the zircons have oscillatory growth zoning with rare sector zoning. Fifteen analyses of zircons have highly varied abundances of ^{232}Th (139-1626 ppm) and ^{238}U (177-1862 ppm) with Th/U ratios ranging from 0.75 to 1.51. Analyses are concordant with a weighted mean $^{206}\text{Pb}/^{238}\text{U}$ age of 301 ± 3 Ma (MSWD=0.89) (Fig. 4c). This dating is identical within error and represents between Lower Permian and Upper Carboniferous.

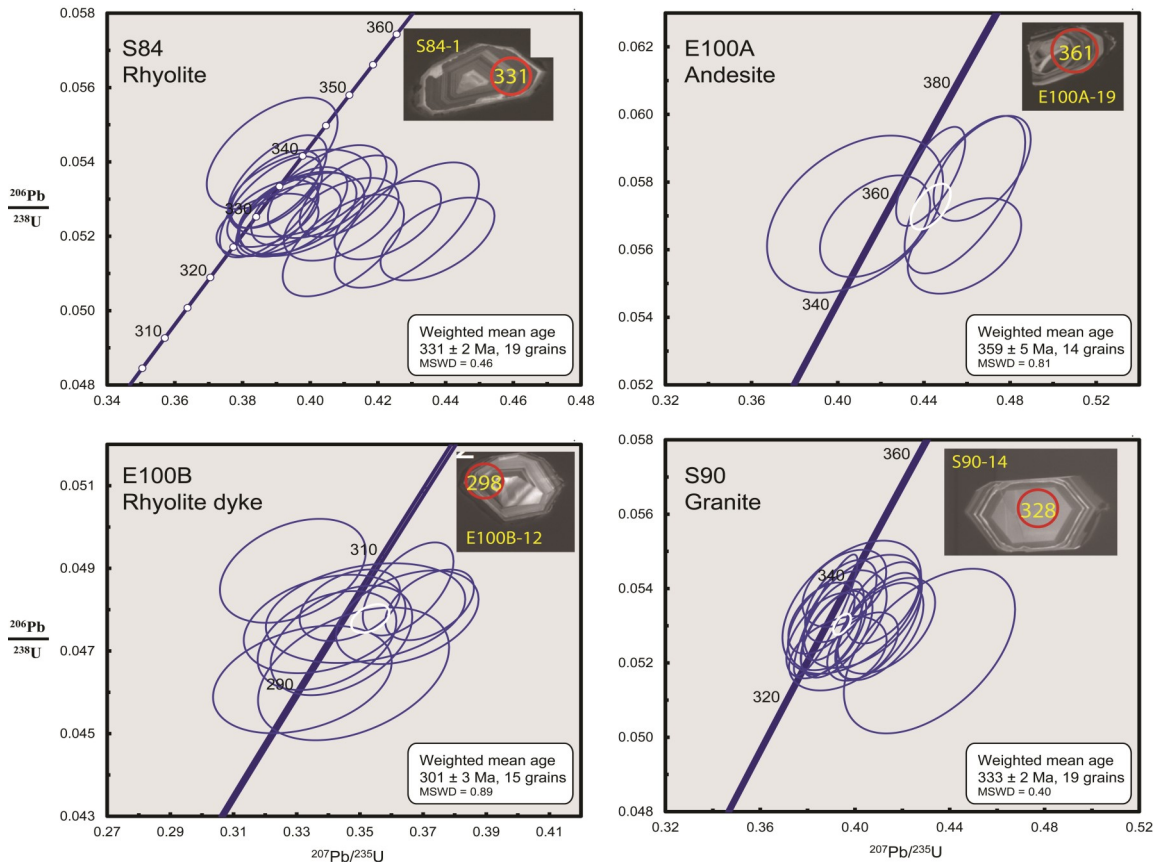


Fig. 4. U-Pb Concordia diagrams for studied volcanic and plutonic rocks from Edren range with dated representative cathodoluminescence (CL) images of zircon grains and weighted mean $^{206}\text{Pb}/^{238}\text{U}$ ages.

The rhyolite sample (S84) from Ulziitkhar Formation in the DK unit has subhedral to euhedral zircons that are 35 μm to 150 μm long and have length/width ratios of between 1:1 and 3:1. The zircons have Th/U ratios of 0.30-1.12, varied abundances of ^{232}Th (83-755 ppm) and ^{238}U (280-935 ppm). Zircons have mainly oscillatory zoning pattern with rare sector zoning. Nineteen analyses from sample S84 yield concordant $^{206}\text{Pb}/^{238}\text{U}$ age of Lower Carboniferous 331 ± 2 Ma (MSWD=0.46) (Fig. 4a).

The granite sample S90 from Bayan-Airag complex chosen to date due to close to the dated rhyolite sample (S84) along the section. Dated granite has subhedral to euhedral zircons that are 40 μm to 200 μm long and have length/width ratios of between 1:1 and 4:1. The zircons have Th/U ratios of 0.30-1.12, varied abundances of ^{232}Th (83-755 ppm) and ^{238}U (280-935 ppm). Zircons show mainly oscillatory zoning pattern with rare sector zoning. Nineteen analyses from sample S90 yield concordant $^{206}\text{Pb}/^{238}\text{U}$ age of Lower Carboniferous 333 ± 2 Ma (MSWD=0.40) (Fig. 4d).

Whole rock chemical compositions

All whole-rock compositions of the representative samples are summarized in Table

1 and 2. Field and petrographic observations revealed evidence of varying degrees of alteration marked by the presence of epidote, chlorite, sericite and carbonates (Fig. 3). Therefore, we used the loss of ignition (LOI) as an indicator for the alteration process and excluded all samples exceeding approximately 4.0 wt% LOI. Trace elements of HFSE and REE have employed that are thought to be relatively immobile during alteration or greenschist to amphibolite-facies metamorphism (e.g., Floyd and Winchester, 1975, Winchester and Floyd, 1977; Pearce, 1996, 2008; Tasáryová et al., 2018).

Major-elements

The TAS diagram shows that the Early Carboniferous volcanic rocks range in composition characteristics of basalt, basaltic andesite, basaltic trachyandesite, andesite, trachyandesite, dacite, and rhyolite and the Late Carboniferous dyke system of rhyolite (Fig. 5a). Basalt, basaltic andesite, basaltic trachyandesite rocks from EN and DK units display a similar range of SiO_2 abundances (47.16-52.13 wt%), narrow TiO_2 (0.60-0.99 wt%), Al_2O_3 (13.81-18.71 wt%), MgO (2.20-7.01 wt%) and $\text{Fe}_2\text{O}_3\text{t}$ (8.40-13.52 wt%) contents. The analyses are also characterized by enrichments in Na_2O over

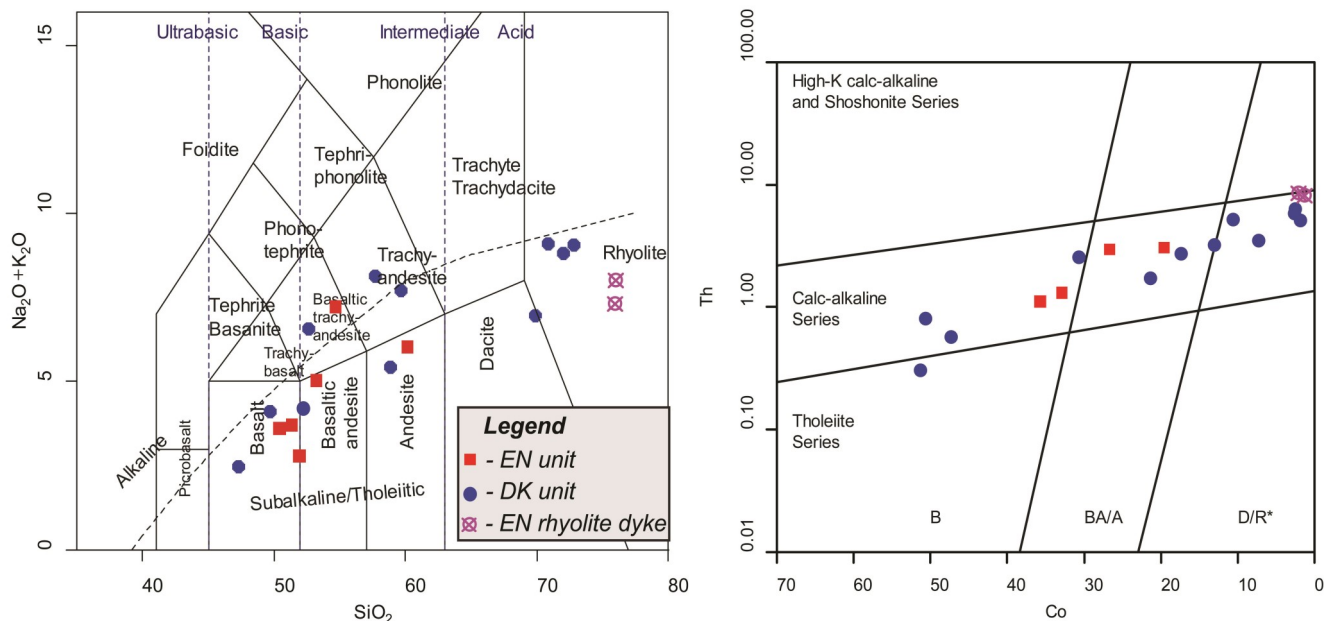


Fig. 5. Classification diagrams for volcanic rocks from the Edren range. (a) SiO_2 vs. $(\text{Na}_2\text{O} + \text{K}_2\text{O})$ diagram of Le Bas et al. (1986); (b) Co-Th binary plot Hastie et al. (2007). Abbreviations: B=basalt; BA/A=basaltic andesite and andesite; D/R*=dacite and rhyolite.

Table 1. Result of major-element geochemical analysis (wt.%)

| | E110 | E111 | E99 | E100A | E100B | E102B | S86C | S86B | S86A | E95 | E94 | E119 | E97A | S84 | S85A | S85B |
|---------------------------------|--------|--------|--------|----------|-------|-------|--------|--------|--------|----------|----------|----------|----------|----------|----------|----------|
| Locality | EN | EN | EN | EN | EN | EN | DK | DK | DK | DK | DK | DK | DK | DK | DK | DK |
| Petrology | basalt | basalt | basalt | andesite | dyke | dyke | basalt | basalt | basalt | andesite | andesite | andesite | rhyolite | rhyolite | rhyolite | rhyolite |
| SiO ₂ | 49.39 | 50.45 | 52.13 | 57.65 | 75.86 | 75.7 | 47.16 | 48.83 | 52.04 | 56.92 | 57.96 | 58.24 | 67.61 | 71.19 | 72.76 | 70.43 |
| Fe ₂ O _{3t} | 12.87 | 11.68 | 10.44 | 7.08 | 12.2 | 12.56 | 13.52 | 10.84 | 8.4 | 8.47 | 8.42 | 7.3 | 4.33 | 3.23 | 2.19 | 2.8 |
| Al ₂ O ₃ | 16.52 | 16.42 | 18.71 | 15.91 | 0.08 | 0.08 | 13.81 | 15.28 | 17.12 | 16.78 | 17.58 | 17.83 | 12.35 | 14.06 | 14.46 | 15.01 |
| TiO ₂ | 0.6 | 0.75 | 0.67 | 0.87 | 0.05 | 0.04 | 0.78 | 0.99 | 0.87 | 0.55 | 0.58 | 0.85 | 0.52 | 0.18 | 0.19 | 0.26 |
| MnO | 0.18 | 0.21 | 0.14 | 0.09 | 0.27 | 0.49 | 0.22 | 0.19 | 0.19 | 0.13 | 0.1 | 0.08 | 0.17 | 0.06 | 0.05 | 0.07 |
| CaO | 10.41 | 9.96 | 8.43 | 4.48 | 0.13 | 0.1 | 14.5 | 11.56 | 10.16 | 4.96 | 5.49 | 3.96 | 4.66 | 1.03 | 0.9 | 1.22 |
| MgO | 4.21 | 4.72 | 2.2 | 3.46 | 4.4 | 3.82 | 7.01 | 6.33 | 3.21 | 2.6 | 2.82 | 1.35 | 0.11 | 0.37 | 0.3 | 0.44 |
| Na ₂ O | 2.21 | 1.96 | 2.84 | 4.91 | 2.89 | 4.17 | 1.58 | 2.45 | 4.07 | 3.66 | 3.24 | 4.68 | 6.32 | 3.29 | 3.58 | 4.23 |
| K ₂ O | 1.32 | 0.75 | 2.1 | 0.86 | 0.02 | 0.02 | 0.89 | 1.62 | 2.45 | 4.4 | 2.12 | 2.86 | 0.42 | 5.45 | 5.5 | 4.85 |
| P ₂ O ₅ | 0.19 | 0.25 | 0.29 | 0.55 | 3.86 | 2.64 | 0.26 | 0.29 | 0.39 | 0.28 | 0.28 | 0.48 | 0.3 | 0.06 | 0.05 | 0.09 |
| LOI | 2.08 | 2.79 | 1.96 | 4.09 | 0.14 | 0.29 | 0.18 | 0.83 | 1.25 | 1.15 | 1.31 | 2.28 | 3.18 | 1 | 0.98 | 1.13 |
| TOTAL | 99.99 | 99.93 | 99.91 | 99.95 | 99.9 | 99.9 | 99.91 | 99.21 | 100.13 | 99.9 | 99.89 | 99.91 | 99.97 | 99.92 | 100.96 | 100.52 |

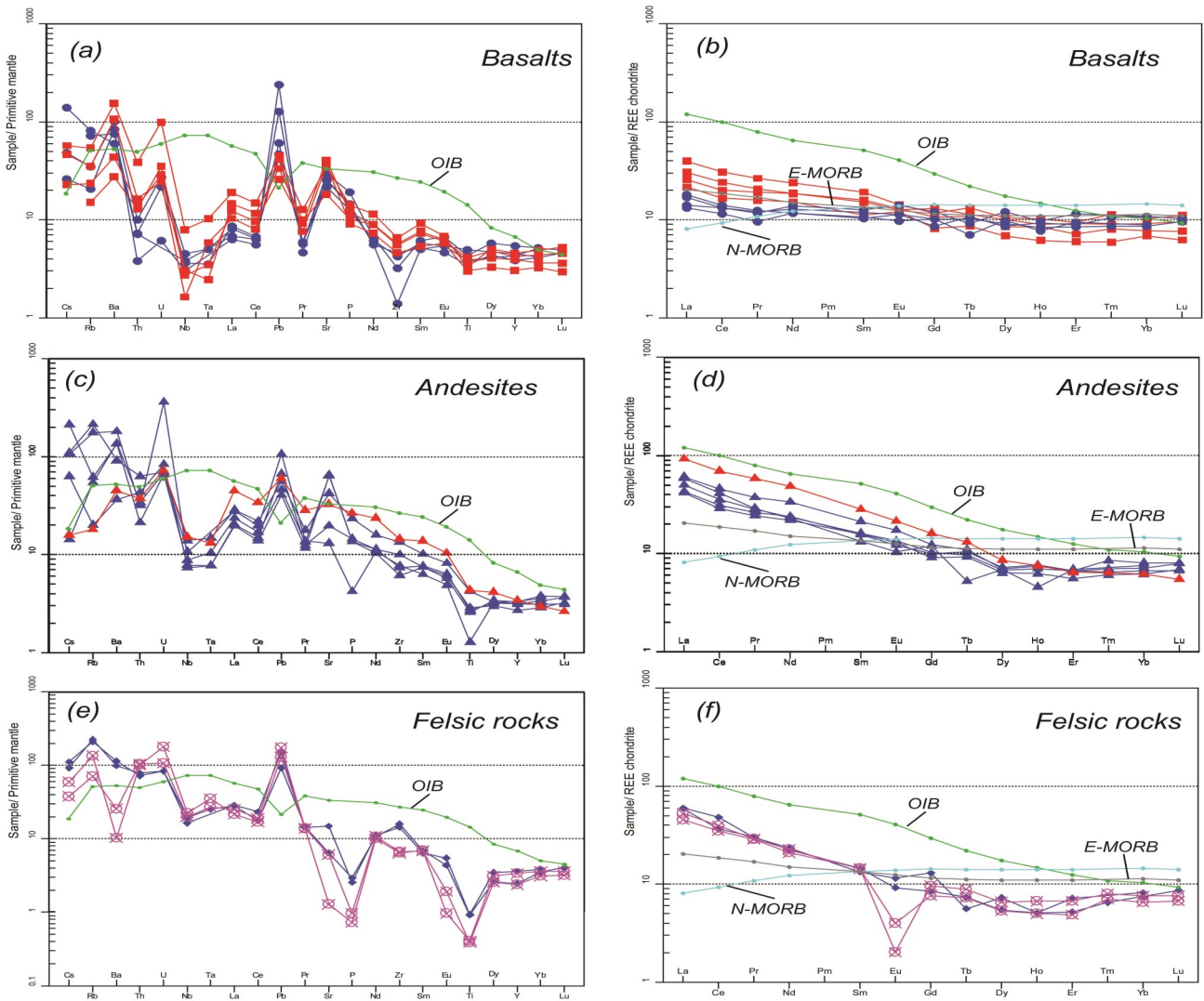


Fig. 6. Spider plots for volcanic rocks from Edren range; (a, c, e) NMORB-normalized trace element patterns (Sun and McDonough, 1989) for presumably little mobile/immobile elements as proposed by Pearce (2014). (b, d, f) Chondrite-normalized (Boynnton, 1984) REE patterns.

K_2O ($Na_2O/K_2O=1.35-2.63$ by weight) at moderate total alkali contents ($Na_2O+K_2O=2.47-6.52$ wt%). The $Mg\#$ [$100 \times MgO/(MgO+FeO)$ {mol.%}] range of DK unit is relatively higher range (41-51) than EN unit (27-42). Andesite, trachyandesite, and trachyte from EN and DK units ($SiO_2=56.92-58.24$ wt%) contain 0.55-0.87 wt% TiO_2 , 15.91-18.00 wt% Al_2O_3 , and higher total alkalis (5.36-8.06 wt%). Na_2O/K_2O ratio of EN unit (5.70) much higher than DK unit (0.83-1.64). Rhyolites from DK unit ($SiO_2=67.61-72.76$ wt%) display on average the lowest TiO_2 (0.18-0.52 wt%), Al_2O_3 (12.35-15.01 wt%), and the ferromagnesian components ($MgO=0.11-0.44$ wt%, $Fe_2O_3=2.19-4.33$ wt%; $Mg\#=5-24$).

The alkalis are ($Na_2O+K_2O=6.74-9.08$ wt%) with extremely changeable Na_2O/K_2O ratios (0.60-15.05) most likely reflecting variable alteration of the individual samples. Two samples of rhyolite dykes in the EN unit were analyzed and they display a limited range of SiO_2 abundances (75.70-75.86 wt%), similar TiO_2 (0.08 wt%), narrow Al_2O_3 (12.20-12.56 wt%), and ferromagnesian ($MgO=0.10-0.13$ wt%, $Fe_2O_3=2.64-3.86$ wt% and $Mg\#=6-7$). Total alkalis display a range of 7.29-7.99 wt% with Na_2O/K_2O ratio vary from 0.92-1.52.

Trace-elements

In a diagram of Hastie et al. (2007), more resistant to the alteration effects than the original

SiO₂-K₂O plot of Peccerillo and Taylor (1976), all samples show a clear normal-K calc-alkaline affinity (Fig. 5b). The trace-element compositions were plotted into NMORB-normalized multi-element diagrams (Sun and McDonough, 1989) (Figs. 6 a,c, and e). Following Pearce (2014), only the presumably immobile or little mobile elements are shown. The multi element patterns of basalts from DK unit less differentiated than basalts from EN unit (Fig. 6a). In addition, both basalts from DK and EN units are characterized by often pronounced negative anomalies in High-Field Strength Elements (HFSE; e.g. Nb, Ta, Ti, Zr, and Hf). Thorium content of EN unit (1.11-3.07 ppm) is significantly higher than the DK unit (0.30-0.80 ppm).

The multi-element patterns of andesites from both EN and DK units are relatively steeper than basalts, also enriched in incompatible elements. The pronounced negative anomalies in HFSE (Nb, Ta, Ti, Zr, and Hf) also observed (Fig. 6c). The multi-element patterns of rhyolite dykes from the EN unit and rhyolites from the DK unit are also relatively similar patterns with andesites from both EN and DK units (Fig. 6e).

The chondrite-normalized (Boynnton, 1984) REE patterns of basalts from the EN unit (Fig. 6b) show significant enrichment (La/Yb)_N=3.24-3.96 in the Light Rare Earth Elements (LREE) relative to the heavy ones (HREE) comparing to basalts from DK unit which show relatively flat pattern (La/Yb)_N=1.34-1.61. The LREE segments of basalts from the EN unit are relatively fractionated as well (La/Sm)_N=1.62-2.07 comparing to basalts from the DK unit (La/Sm)_N=1.11-1.40.

The chondrite-normalized REE patterns of andesite from the EN unit (Fig. 6d) (La/Yb)_N=15.39 show more enrichment in the LREE comparing to andesites from DK unit (La/Yb)_N=6.87-10.91. Steeper LREE patterns of andesites from EN and DK units show relative to mainly flat HREE. The LREE segments of andesite from the DK unit are relatively fractionated as well (La/Sm)_N=2.64-4.62.

The chondrite-normalized REE patterns of rhyolite dykes from EN unit and rhyolites from DK show (Fig. 6f) similar and significant enrichment (La/Yb)_N=5.47-8.24 in the LREE

relative to the relatively flat HREE. The LREE segments rhyolites from DK unit are relatively fractionated as well (La/Sm)_N=2.73-4.50 comparing to rhyolite dykes from EN unit (La/Sm)_N=3.10-3.67. Depletion of Eu only observed in samples of rhyolite dykes in the EN unit.

Sr and Nd isotopes

The Sm-Nd isotopic data for 8 samples are listed in Table 3, and the initial εNd-values are compared with published data of the adjacent similar Carboniferous volcanic formations in the CAOB. The initial εNd-values for two basalts (samples of E99, E110) from EN unit were estimated based on U-Pb age of andesite (sample E100A) from EN unit and they exhibit a spectrum of initial εNd-values from ca. +1.9 to +4.3 (Fig. 7) with initial (⁸⁷Sr/⁸⁶Sr)₃₅₉ ratio of 0.704158-0.704332 and initial ¹⁴³Nd/¹⁴⁴Nd₃₅₉ ratios from 0.512272 to 0.512393. They have Neoproterozoic two-stage Nd depleted mantle model ages of 0.732-0.918 Ga. The basalt sample E110 from Lower Devonian Ulgii Formation reported for an age of ca. 410 Ma based on paleontological data (Togtokh et al., 2020). The εNd-values for sample E110 estimated based on age at 359 Ma (+4.3) and at ca. 410 Ma (+4.5) produced not a significant error. The ages of respective ages for 360 Ma and ca. 410 Ma for sample E110 are 0.732 Ga and 0.752 Ga, respectively.

The initial εNd-values for samples from the DK unit were estimated based on U-Pb ages of rhyolite (sample S84) and granite (sample S90) from the DK unit and they exhibit a spectrum of initial εNd-values from ca. +1.6 to +5.8 (Fig. 7). The initial εNd-values for basalt (S86C) from DK unit exhibit highest spectrum of an initial εNd-value of ca. +5.8 with initial (⁸⁷Sr/⁸⁶Sr)₃₅₉ ratio of 0.704754 and initial (¹⁴³Nd/¹⁴⁴Nd)₃₅₉ ratios from 0.512510. It has Neoproterozoic two-stage Nd depleted mantle model ages of 0.589 Ga. The εNd-values for andesites (sample E95) from DK unit exhibit also show spectrum of ca. from +1.6 (Fig. 7) with an initial (⁸⁷Sr/⁸⁶Sr)₃₅₉ ratio of 0.704939 and an initial (¹⁴³Nd/¹⁴⁴Nd)₃₅₉ ratio of 0.512295. It has Neoproterozoic two-stage Nd depleted mantle model age of 0.919 Ga.

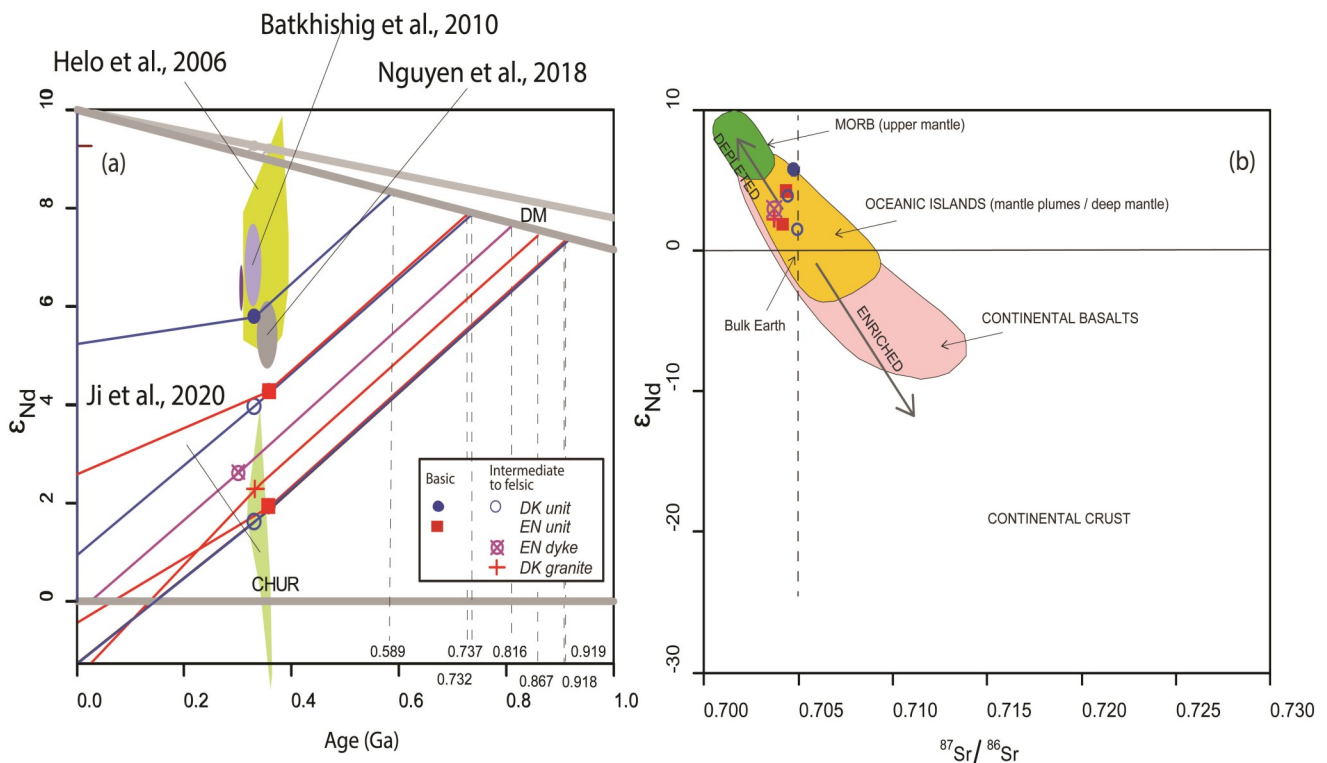


Fig. 7. Neodymium evolution diagram of volcanic rocks in the Edren range; T_{DM}^{Nd} : two-stage crustal model age. Previously published data (Helo et al., 2006; Batkhishig et al., 2010; Nguyen et al., 2018) of volcanic rocks from southern Mongolia were also plotted in a diagram.

The U-Pb age of 331 Ma obtained for rhyolite sample S84 from DK give ($^{87}Sr/^{86}Sr$)₃₃₁ ratio of 0.704448 and initial ($^{143}Nd/^{144}Nd$)₃₅₉ ratio of 0.512414. It is characterized by a positive ϵ_{Nd} -value of +3.9 (Fig. 7) and has Neoproterozoic age of 0.737 Ga. The granite sample S90 from DK unit gives ($^{87}Sr/^{86}Sr$)₃₃₁ ratio of 0.703788 and initial ($^{143}Nd/^{144}Nd$)₃₅₉ ratio of 0.512329. It is characterized by a positive ϵ_{Nd} -value of +2.3 and has Neoproterozoic age of 0.867 Ga.

The U-Pb age of 301 Ma obtained for the rhyolite porphyry sample E100B from dyke cross-cutting andesite outcrop near sample E100A gives ($^{87}Sr/^{86}Sr$)₃₃₁ ratio of 0.704209 and initial ($^{143}Nd/^{144}Nd$)₃₅₉ ratio of 0.512385. It is characterized by a positive ϵ_{Nd} -value of +2.6 (Fig. 7) and has Neoproterozoic age of 0.816 Ga.

DISCUSSION AND CONCLUSION

Timing of magmatism

Three episodes of magmatism can be recognized in the Edren range. The earliest episode of magmatism at c. 360 Ma is dated in the EN unit,

whereas younger episode of magmatism at c. 330 Ma was dated in the DK unit. The youngest episode of magmatism at c. 300 Ma dated in the EN unit as a formation of rhyolite porphyry dykes. Obtained ages of c. 360 Ma and c. 330 Ma in this study are correspond with previously reported age ranges of arc-related volcanic rocks (c. 350-326 Ma; Nguyen et al., 2018) and plutonic rocks (c. 356-330 Ma; Yarmolyuk et al., 2008; Cai et al., 2014).

Alteration effects

The volcanic rocks from EN and DK units of the Edren range have been altered to various degrees based on the petrographic observation (Fig. 3) and some of the samples have high LOI (up to 4.09 wt%) (Table 1). Most of the incompatible elements such as Rb, Ba, K, and Cs are considered to be mobile during the metamorphic alteration (Hastie et al., 2007; Pearce and Cann, 1973). Therefore, in the discussion part, we used immobile elements such as REEs, Th, Nb, Ta, Y and Sr-Nd isotopes.

Table 3. Whole-rock Sr–Nd isotopic compositions for volcanic and plutonic rocks from Edren range, Trans–Altai Zone.

| Sample | Rock type | Geological setting | Rb | Sr | Sm | Nd | $^{87}\text{Rb}/^{86}\text{Sr}$ | $^{147}\text{Sm}/^{144}\text{Nd}$ | Age (Ma) | $^{87}\text{Sr}/^{86}\text{Sr}_i$ | $^{143}\text{Nd}/^{144}\text{Nd}_i$ | ϵNd_i | $T_{\text{DM}}(\text{Ga})$ |
|--------|---------------|--------------------|-----|------|----|----|---------------------------------|-----------------------------------|----------|-----------------------------------|-------------------------------------|-----------------------|----------------------------|
| E110 | Basalt | EN unit | 21 | 754 | 3 | 10 | 0.0803 | 0.1599 | 360 | 0.70433 | 0.512393 | 4.3 | 0.732 |
| E99 | Basalt | EN unit | 32 | 658 | 3 | 13 | 0.1421 | 0.1454 | 360 | 0.70416 | 0.512272 | 1.9 | 0.918 |
| S86C | Basalt | DK unit | 22 | 430 | 2 | 7 | 0.148 | 0.1839 | 330 | 0.70475 | 0.51251 | 5.8 | 0.589 |
| E95 | Andesite | DK unit | 105 | 1151 | 2 | 12 | 0.2639 | 0.1286 | 330 | 0.70494 | 0.512295 | 1.6 | 0.919 |
| S84 | Rhyolite | DK unit | 137 | 132 | 2 | 11 | 2.9956 | 0.1154 | 330 | 0.70445 | 0.512414 | 3.9 | 0.737 |
| S90 | Granite | DK unit | 128 | 271 | 1 | 8 | 1.373 | 0.1062 | 330 | 0.70379 | 0.512329 | 2.3 | 0.867 |
| E100B | Rhyolite dyke | EN unit | 48 | 122 | 2 | 12 | 1.1323 | 0.1224 | 300 | 0.70423 | 0.512386 | 2.6 | 0.816 |

Geotectonic environment and petrogenesis

In the Th-Hf/3-Ta ternary plot of Wood (1980) basalts from EN and DK units fall in the Calc-Alkaline Basalts (CAB) field (Fig. 8a). In the Zr/4-2Nb-Y discrimination diagram of Meschede (1986), basalts from EN and DK units plot into the fields D, suggesting volcanic-arc basalts (Fig. 8b). One sample plotted outside of D field due to enrichment in Y. In the Nb/La-La/Yb and Th/Nb-La/Yb binary plots of Hollocher et al. (2012), the clear compositional gap between basalts from EN and DK units (Figs. 8c and d). Basalts from EN unit plotted in the Continental arcs field, in contrast, basalts from DK unit closer to Oceanic arcs field. This gap between EN and DK basalts reflects in their geochemical character. Basalts from EN unit have lower Mg# values (27-42), MgO (2.20-4.72 wt%), Cr (19-43 ppm), Ni (21-46 ppm) contents, and higher enrichment in Th (1.11-3.07 ppm) and LREE than basalts from DK unit. In contrast, basalts from the DK unit have higher Mg# values (41-51), MgO (3.21-7.01 wt%), Cr (260-408 ppm), Ni (128-144 ppm), lower content of Th (0.30-0.80 ppm). Both basalts from EN and DK have a flat pattern of HREE, but DK basalts less fractionated (La/Yb=1.9-2.3) than EN basalts (La/Yb=4.7-5.7), close to MORB signature. Furthermore, both EN and DK basalts have relatively strong positive initial ϵNd -values (from ca. +1.9 to +5.8) which could reflect a direct contribution of mantle magma source in subduction zone (Fig. 7) (DePaolo, 1981; Jahn et al., 2000). Higher Th/Nb (0.6-1.2), U/Nb (0.3-0.5) and lower Nb/La (0.2-0.4) ratios for basalts from EN unit indicate subduction fluids input of magma source (Figs. 9a and b) (Hofmann, 1997; Wang et al., 2016). In contrast, for basalts from DK unit, lower Th/Nb (0.2-0.3), U/Nb (0.1-0.2) and higher Nb/La (0.5-0.6) ratios were defined. This indicates subduction fluids input to the basaltic magma source is much negligible. Furthermore, in the Th/Zr vs Th/Nb diagram (Fig. 9c) for mixing modelling, most of basalts from EN unit tend to along the mixing line between depleted mantle and sedimentary melt from the subducted slab (Tatsumi, 2001) except one sample, indicating source of mixing (within 10-20% recycled crust). In other hand, basalts from

DK unit has limited source of mixing (~10% UCC or ~5% recycled crust), comparing to basalts from EN unit (Fig. 9c). In the La/Yb vs Dy/Yb diagram (Fig. 9e), most of basalts from both EN and DK units are concentrated close to the trend of the partial melting of spinel peridotite facies from a relatively shallow source (Jung et al., 2006). In addition, basalts from EN and DK units plot mainly along with the trend of partial melting but not fractional crystallization on the La/Sm vs La diagram (Fig. 9d) (Allegre and Minster, 1978). All these above suggest that the geochemical characters of basalts and andesite from EN unit can be derived from partial melting of a contaminated mantle wedge. Whereas basalts from DK unit can be derived from partial melting of the relatively uncontaminated mantle wedge.

Rhyolite from DK unit display a Volcanic Arc Granites (VAG) character in the Nb-Y binary diagram of Pearce et al. (1984) and Hf-Rb-Ta discrimination diagram (Harris et al., 1986) (Figs. 8e and f). The coeval (c. 330 Ma) rhyolites and granite from the DK unit display positive initial ϵNd -values (+3.9 and +2.3, respectively) different from interbedded basalt and andesite (+5.8 and +1.6, respectively) (Fig. 7), suggesting a different magma source for them.

The younger (c. 300 Ma) rhyolite porphyry dyke cross-cutting andesite developed in EN unit show positive ϵNd -value of +2.6 and Neoproterozoic age of 0.816 Ga, similar with granite from the DK unit. Comparing to rhyolites from the DK unit, rhyolite porphyry dyke in the EN unit has chondrite-normalized REE and NMORB-normalized trace element patterns displaying more evidently negative Eu and Ti anomalies (Fig. 6). This indicates that fractional crystallization is dominated by plagioclase and Ti-bearing minerals (e.g., rutile). In the Hf-Rb-Ta discrimination diagram (Harris et al., 1986), rhyolite porphyry dykes from EN unit plotted in the fields of group 3 (post-collision granite) and within-plate granite (Fig. 8f).

Geodynamic implication

The geodynamic setting of SW Mongolia can be characterized by from Early Neoproterozoic to

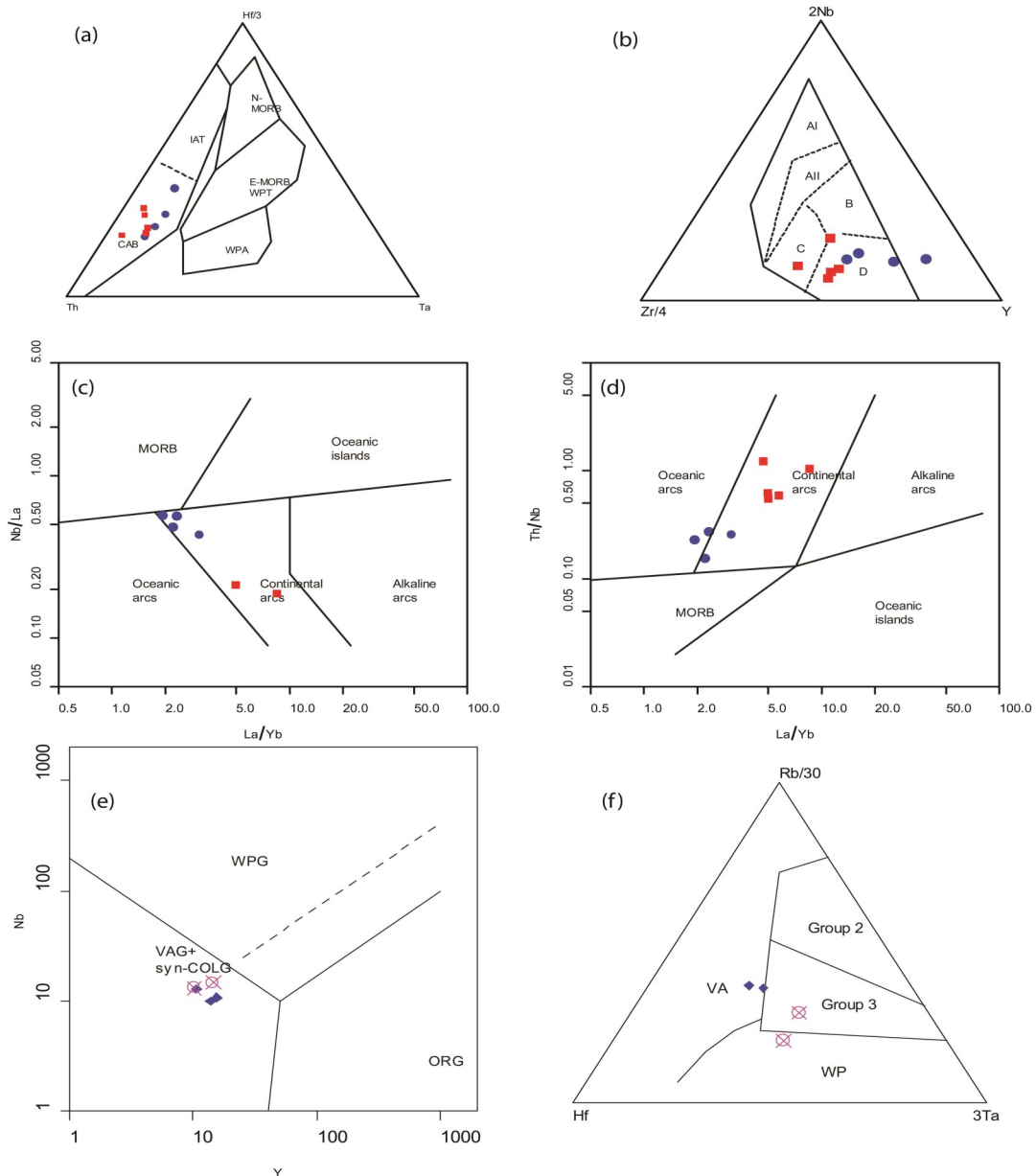


Fig. 8. Geotectonic discrimination diagrams for volcanic and plutonic rocks from Edren range; (a) Th-Hf/3-Ta triangular plot of Wood (1980); CAB=Calc-Alkaline Basalts; IAT=Island-Arc Tholeiites; WPT=Within Plate Tholeiites; WPA=Within Plate Alkaline basalts; (b) Zr/4-2Nb-Y triangular plot of Meschede (1986) for basic rocks. AI-AII=Within Plate Alkaline basalts; B=P-type mid-ocean ridge basalts; C-D=Volcanic arc basalts; (c-d) La/Yb-Nb/La and La/Yb-Th/Nb plots of Hollocher et al. (2012); (e) Nb-Y plot of Pearce et al. (1984); (f) Hf-Rb-Ta discrimination diagram (Harris et al., 1986). The symbols are the same as Fig. 5.

Late Paleozoic subduction-accretionary collage of metamorphic and magmatic zones from north to southward formed a juvenile crust (Buriánek et al., 2017, Kozlovsky et al., 2015; Kröner et al., 2014; Jiang et al., 2017). Three main magmatic peak events (Cambrian, Devonian and Early Carboniferous) occurred by subduction of, steady oceanic retreating (Janoušek et al., 2018;

Hanžl et al., 2016). The Cambrian event created the gigantic Ikh-Mongol Arc System (Janoušek et al., 2018) whose juvenile material was under thrustured beneath the Trans-Altai Zone during the Late Devonian-Early Carboniferous shortening period (Lehmann et al., 2010; Guy et al., 2014). Subsequently, a massive Devonian arc-type

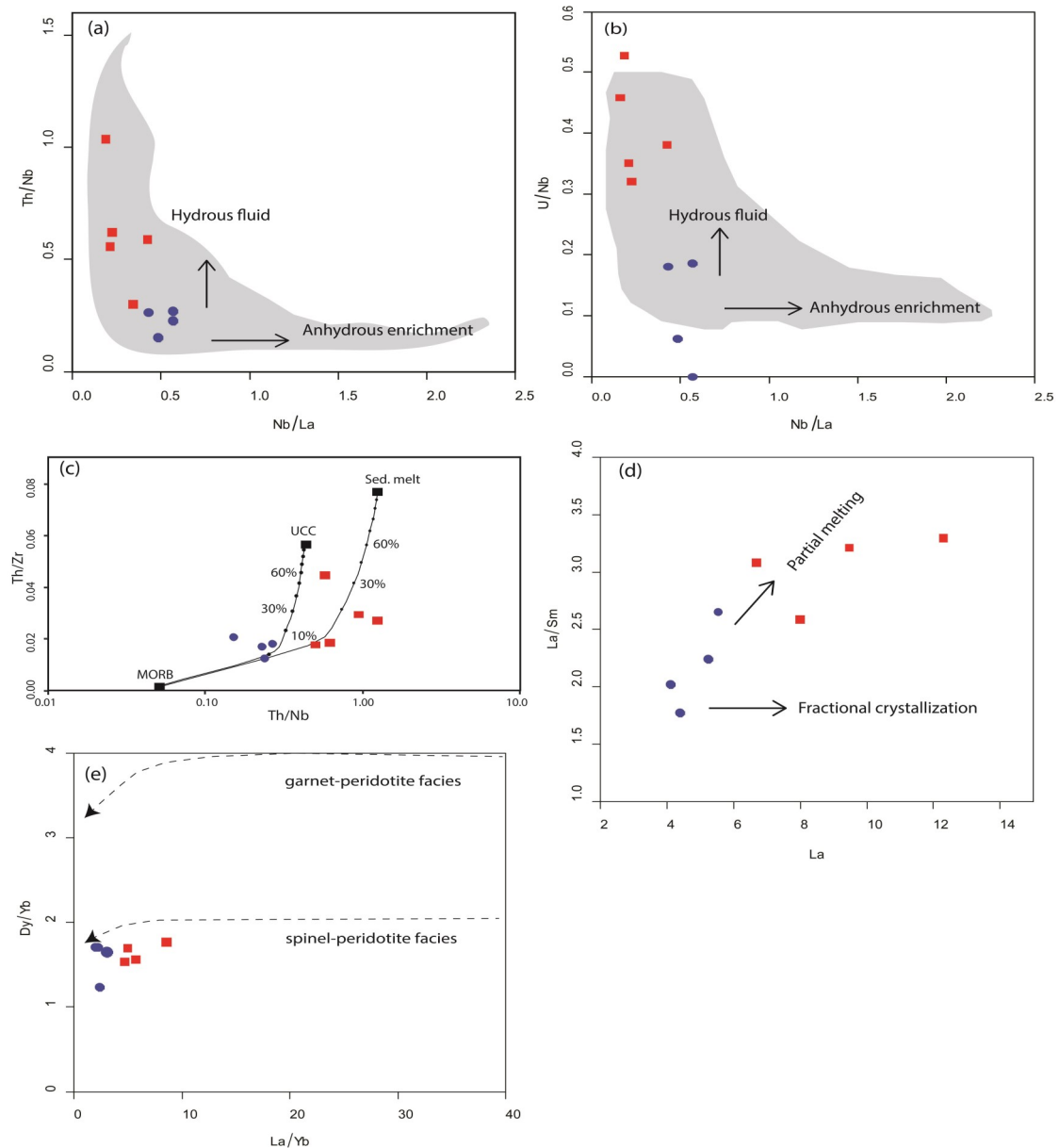


Fig. 9. Petrogenetic diagram for the volcanic rocks from Edren range; (a and b) Nb/La-Th/Nb and Nb/La-U/Nb plots for basalts from Edren range. The trends suggest the source of arc basalts from the EN unit contains a hydrous component. (c) Mixing modelling Th/Zr versus Th/Nb diagram for a compositional range between depleted mantle source and recycled crustal substrate (d) La-La/Sm diagram of Allègre and Minster (1978); (e) Dy/Yb vs. La/Yb plots for basalts from Edren range. Trends of the spinel peridotite and garnet-peridotite facies in (e) are from (Jung et al., 2006). The symbols are the same as Fig. 5.

magmatism developed within the Gobi-Altai Zone and Chinese Altai zones with a peak between 400 and 370 Ma, constrained by dating of arc-type gabbroid and granitoid (Cai et al., 2011, 2015; Hanžl et al., 2016; Yuan et al., 2007; Munkhtsengel et al., 2018).

Trans-Altai zone considered to be built by Early Carboniferous arc volcanism (Cai et al., 2014;

Nguyen et al., 2018) and Late Paleozoic back-arc or rifting (Zhu et al., 2017; Yarmolyuk et al., 2008). Two pulses of subduction related Mississippian volcanism, i.e. c. 360 Ma (EN unit) and c. 330 Ma (DK unit) can be recognized in the Edren range of Trans-Altai Zone. The first pulse of c. 360 Ma continental arc volcanism produced relatively contaminated basalt-

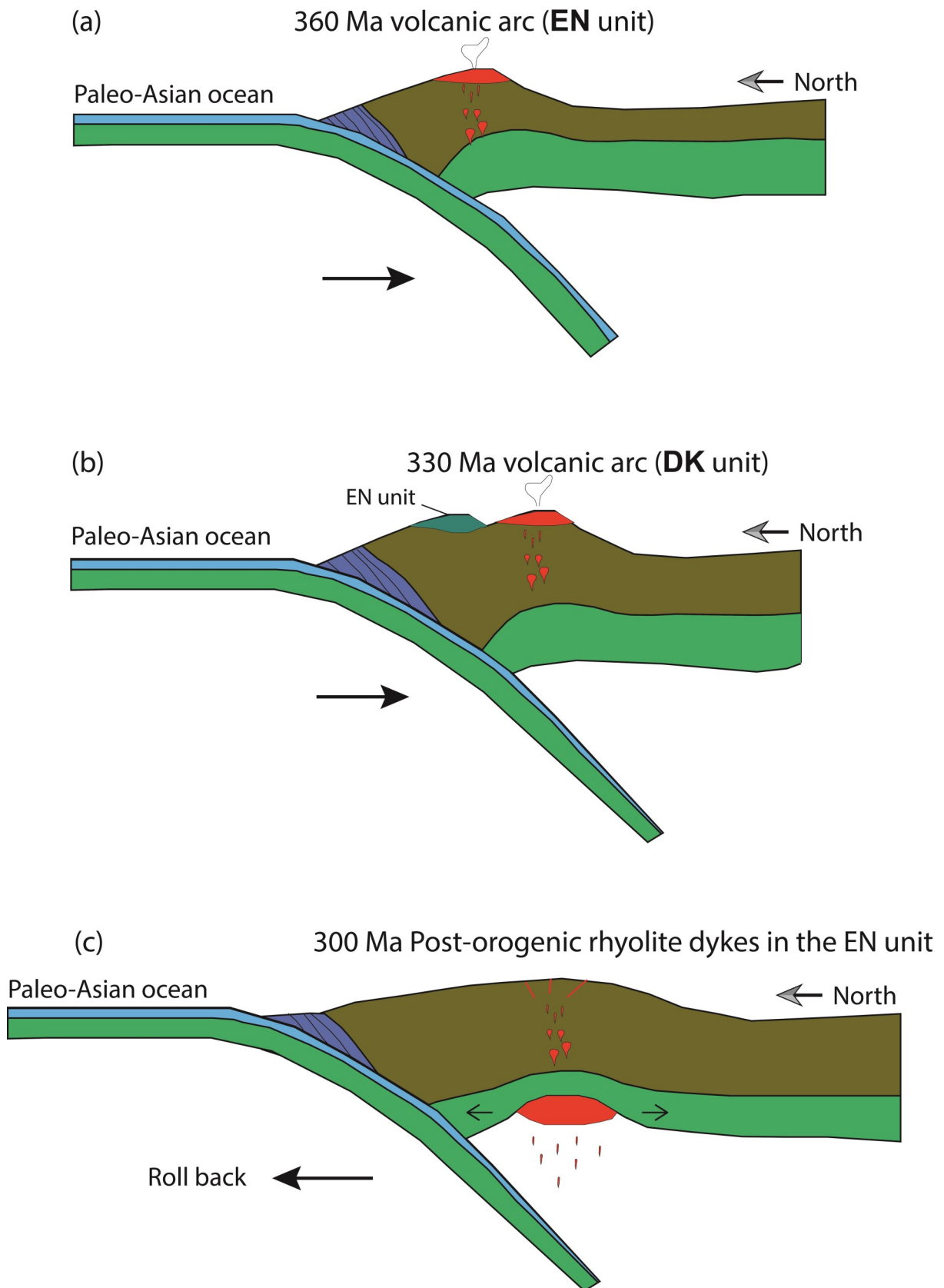


Fig. 10. Schematic diagram showing the tectonic evolution of Edren range, Trans-Altai, SW Mongolia

andesite magma with lower initial ϵNd -values by subduction of the oceanic crust, developed on Devonian continental juvenile crust (Fig. 10a). Following subduction, steady northward transition of volcanic arc had occurred. At c. 330 Ma continuous subduction of oceanic crust produced basalt-andesite-rhyolite magma with higher ϵNd -values (Fig. 10b). During the c. 300 Ma, rhyolite porphyry dykes developed in the EN unit by post-orogenic magmatism (Fig. 10c).

ACKNOWLEDGEMENTS

We are grateful to Liu Yifei and Si-Hong Jiang for their useful comments and discussion. We also thank D.Tsendbazar who helped us with the sampling and fieldwork. This research was financially supported by the Mongolian Foundation for Science and Technology (No.ShUTT_012/2015) and Chinese Geological Survey (No.DD20190437).

REFERENCES

- Allegre, C.J., Minster, J.F. 1978. Quantitative models of trace element behavior in magmatic processes. *Earth and Planetary Science Letters*, v. 38(1), p. 1-25. [https://doi.org/10.1016/0012-821X\(78\)90123-1](https://doi.org/10.1016/0012-821X(78)90123-1)
- Badarch, G., Cunningham, W.D., Windley, B.F. 2002. A new terrane subdivision for Mongolia: implications for the Phanerozoic crustal growth of Central Asia. *Journal of Asian Earth Sciences*, v. 21(1), p. 87-110. [https://doi.org/10.1016/S1367-9120\(02\)00017-2](https://doi.org/10.1016/S1367-9120(02)00017-2)
- Batkhisig, B., Noriyoshi, T., Greg, B. 2010. Magmatism of the Shuteen Complex and Carboniferous subduction of the Gurvansaikhan terrane, South Mongolia. *Journal of Asian Earth Sciences*, v. 37(5-6), p. 399-411. <https://doi.org/10.1016/j.jseaes.2009.10.004>
- Boynton, W.V. 1984. Cosmochemistry of the rare earth elements: meteorite studies. *Developments in Geochemistry*, v. 2, p. 63-114. <https://doi.org/10.1016/B978-0-444-42148-7.50008-3>
- Buriánek, D., Schulmann, K., Hrdličková, K., Hanžl, P., Janoušek, V., Gerdes, A., Lexa, O. 2017. Geochemical and geochronological constraints on distinct Early-Neoproterozoic and Cambrian accretionary events along southern margin of the Baydrag Continent in western Mongolia. *Gondwana Research*, v. 47, p. 200-227. <https://doi.org/10.1016/j.gr.2016.09.008>
- Cai, K., Sun, M., Xiao, W., Yuan, C., Zhao, G., Long, X., Tumurkhuu, D., Zhou, K. 2017. Petrogenesis of late Paleozoic tholeiitic, Nb-enriched, calc-alkaline and adakitic rocks in southwestern Mongolia: Implications for intra-oceanic arc evolution. *Lithos*, v. 202, p. 413-428. <https://doi.org/10.1016/j.lithos.2014.06.004>
- DePaolo, D.J. 1981. Neodymium isotopes in the Colorado Front Range and crust-mantle evolution in the Proterozoic. *Nature*, v. 291, p. 193-196. <https://doi.org/10.1038/291193a0>
- Floyd, P.A., Winchester, J.A. 1975. Magma type and tectonic setting discrimination using immobile elements. *Earth and Planetary Science Letters*, v. 27(2), p. 211-218. [https://doi.org/10.1016/0012-821X\(75\)90031-X](https://doi.org/10.1016/0012-821X(75)90031-X)
- Gordienko, I.V. 1987. Paleozoic Magmatism and Geodynamics of the Central Asian Fold Belt. Nauka, Moscow, p. 240 (in Russian).
- Guy, A., Schulmann, K., Munschy, M., Mieke, J.M., Edel, J.B., Lexa, O., Fairhead, D. 2014. Geophysical constraints for terrane boundaries in southern Mongolia. *Journal of Geophysical Research: Solid Earth*, v. 119(10), p. 7966-7991. <https://doi.org/10.1002/2014JB011026>
- Hanžl, P., Bat-Ulzii, D., Rejchrt, M., Košler, J., Bolormaa, Kh., Hrdličková, K. 2008. Geology and geochemistry of the Palaeozoic plutonic bodies of the Trans-Altay Gobi, SW Mongolia: Implications for magmatic processes in an accreted volcanic-arc system. *Journal of Geosciences*, v. 53(2), p. 201-234. <https://doi.org/10.3190/jgeosci.028>
- Hanžl, P., Schulmann, K., Janousek, V., Lexa, O., Hrdličková, K., Jiang, Y., Buriánek, D., Altanbaatar, B., Ganchuluun, T., Erban, V. 2016. Making continental crust: origin of Devonian orthogneisses from SE Mongolian Altai. *Journal of Geoscience*, v. 61(1), p. 25-50. <https://doi.org/10.3190/jgeosci.206>
- Harris, N.B., Pearce, J.A., Tindle, A.G. 1986. Geochemical characteristics of collision-zone magmatism. *Geological Society London Special Publications*, v. 19(1), p. 67-81. <https://doi.org/10.1144/GSL.SP.1986.019.01.04>
- Hastie, A.R., Kerr, A.C., Pearce, J.A., Mitchell,

- S.F. 2007. Classification of Altered Volcanic Island Arc Rocks using Immobile Trace Elements: Development of the Th-Co Discrimination Diagram. *Journal of Petrology*, v. 48(12), p. 2341-2357. <https://doi.org/10.1093/petrology/egm062>
- Helo, C., Hegner, E., Kroner, A., Badarch, G., Tomurtogoo, O., Windley, B.F., Dulski, P. 2006. Geochemical signature of Paleozoic accretionary complexes of the Central Asian Orogenic Belt in South Mongolia: constraints on arc environments and crustal growth. *Chemical Geology*, v. 227(3-4), p. 236-257. <https://doi.org/10.1016/j.chemgeo.2005.10.003>
- Hofmann, A.W. 1997. Mantle geochemistry: the message from oceanic volcanism. *Nature*, v. 385(6613), p. 219-229. <https://doi.org/10.1038/385219a0>
- Hollocher, K., Robinson, P., Walsh, E., Roberts, D. 2012. Geochemistry of amphibolite-facies volcanics and gabbros of the Støren Nappe in extensions west and southwest of Trondheim, Western Gneiss Region, Norway: a key to correlations and paleotectonic settings. *American Journal of Science*, v. 312 (4), p. 57-416. <https://doi.org/10.2475/04.2012.01>
- Hou, Z., Yang, Z., Qu, X., Meng, X., Li, Z., Beaudoin, G., Rui, Z., Gao, Y., Zaw, K. 2009. The Miocene Gangdese porphyry copper belt generated during post-collisional extension in the Tibetan Orogen. *Ore Geology Reviews*, v. 36(1-3), p. 25-51. <https://doi.org/10.1016/j.oregeorev.2008.09.006>
- Jackson, S.E., Pearson, N.J., Griffin, W.L., Belousova, E.A. 2004. The application of laser ablation-inductively coupled plasma-mass spectrometry to in situ U-Pb zircon geochronology. *Chemical Geology*, v. 211(1-2), p. 47-69. <https://doi.org/10.1016/j.chemgeo.2004.06.017>
- Jahn, B.M. 2010. Accretionary orogen and evolution of the Japanese Islands: Implications from a Sr-Nd isotopic study of the Phanerozoic granitoids from SW Japan. *American Journal of Science*, v. 310(10), p. 1210-1249. <https://doi.org/10.2475/10.2010.02>
- Jahn, B.M., Windley, B., Natal'in, B., Dobretsov, N. 2004. Phanerozoic continental growth in Central Asia. *Journal of Asian Earth Sciences*, v. 23(5), p. 599-603. [https://doi.org/10.1016/S1367-9120\(03\)00124-X](https://doi.org/10.1016/S1367-9120(03)00124-X)
- Jahn, B.M., Wu, F.Y., Chen, B. 2000. Granitoids of the Central Asian Orogenic Belt and continental growth in the Phanerozoic. *Earth and Environmental Science Transactions of the Royal Society of Edinburgh*, v. 91(1-2), p. 181-193. <https://doi.org/10.1017/S0263593300007367>
- Janoušek, V., Jiang, Y., Buriánek, D., Schulmann, K., Hanzl, P., Soejono, I., Kröner, A., Altanbaatar, B., Erban, V., Lexa, O., Ganchuluun, T., Košler, J. 2018. Cambrian-Ordovician magmatism of the Ikh-Mongol Arc system exemplified by the Khantaishir Magmatic Complex (Lake Zone, south-central Mongolia). *Gondwana Research*, v. 54, p. 122-149. <https://doi.org/10.1016/j.gr.2017.10.003>
- Jian, P., Kröner, A., Jahn, B.M., Windley, B.F., Shi, Y., Zhang, W., Zhang, F., Miao, L., Tumurhuu, D., Liu, D. 2014. Zircon dating of Neoproterozoic and Cambrian ophiolites in West Mongolia and implications for the timing of orogenic processes in the central part of the Central Asian Orogenic Belt. *Earth-Science Reviews*, v. 133, p. 62-93. <https://doi.org/10.1016/j.earscirev.2014.02.006>
- Jiang, Y.D., Schulmann, K., Kröner, A., Sun, M., Lexa, O., Janoušek, V., Buriánek, D., Yuan, C., Hanzl, P. 2017. Neoproterozoic-early Paleozoic peri-Pacific accretionary evolution of the Mongolian collage system: Insights from geochemical and U-Pb zircon data from the Ordovician sedimentary wedge in the Mongolian Altai. *Tectonics*, v. 36(11), p. 2305-2331. <https://doi.org/10.1002/2017TC004533>
- Jung, C., Jung, S., Hoffer, E., Berndt, J. 2006. Petrogenesis of Tertiary Mafic Alkaline Magmas in the Hocheifel, Germany. *Journal of Petrology*, v. 47, p. 1637-1671. <https://doi.org/10.1093/petrology/egl023>
- Kozlovsky, A.M., Yarmolyuk, V.V., Salnikova, E.B., Travin, A.V., Kotov, A.B., Plotkina, J.V., Kudryashova, E.A., Savatenkov, V.M. 2015. Late Paleozoic anorogenic magmatism of the Gobi Altai (SW Mongolia): Tectonic position, geochronology and correlation with igneous activity of the Central Asian Orogenic Belt. *Journal of Asian Earth*

- Sciences, v. 113, p. 524-541.
<https://doi.org/10.1016/j.jseaes.2015.01.013>
- Kröner, A., Kovach, V., Belousova, E., Hegner, E., Armstrong, R., Dolgoplova, A., Seltmann, R., Alexeiev, D.V., Hoffmann, J.E., Wong, J., Sun, M., Cai, K., Wang, T., Tong, Y., Wilde, S.A., Degtyarev, K.E., Rytisk, E. 2014. Reassessment of continental growth during the accretionary history of the Central Asian Orogenic Belt. *Gondwana Research*, v. 25(1), p. 103-125.
<https://doi.org/10.1016/j.gr.2012.12.023>
- Kröner, A., Lehmann, J., Schulmann, K., Demoux, A., Lexa, O., Tomurhuu, D., Štípská, P., Liu, D., Wingate, M.T.D. 2010. Lithostratigraphic and geochronological constraints on the evolution of the Central Asian Orogenic Belt in SW Mongolia: Early Paleozoic rifting followed by late Paleozoic accretion. *American Journal of Science*, v. 310(7), p. 523-574.
<https://doi.org/10.2475/07.2010.01>
- Le Bas, M.J., Le Maitre, R.W., Streckeisen, A., Zanettin, B. 1986. A Chemical Classification of Volcanic Rocks Based on the Total Alkali-Silica Diagram. *Journal of Petrology*, v. 27 (3), p. 745-750.
<https://doi.org/10.1093/petrology/27.3.745>
- Lehmann, J., Schulmann, K., Lexa, O., Corsini, M., Kröner, A., Štípská, P., Tomurhuu, D., Otgonbator, D. 2010. Structural Constraints on the Evolution of the Central Asian Orogenic Belt in SW Mongolia. *American Journal of Science*, v. 310(7), p. 575-628.
<https://doi.org/10.2475/07.2010.02>
- Liu, Y., Gao, S., Hu, Z., Gao, C., Zong, K., Wang, D. 2010. Continental and Oceanic Crust Recycling-induced Melt-Peridotite Interactions in the Trans-North China Orogen: U-Pb Dating, Hf isotopes and Trace Elements in Zircons from Mantle Xenoliths. *Journal of Petrology*, v. 51(1-2), p. 537-571.
<https://doi.org/10.1093/petrology/egp082>
- Ludwig, K.R. 2003. Mathematical-statistical treatment of data and errors for ²³⁰Th/U geochronology. *Reviews in Mineralogy and Geochemistry*, 2003, v. 52(1), p. 631-656.
<https://doi.org/10.2113/0520631>
- Meschede, M. 1986. A method of discriminating between different types of mid-ocean ridge basalts and continental tholeiites with the Nb 1bZr 1bY diagram. *Chemical Geology*, v. 56(3-4), p. 207-218.
[https://doi.org/10.1016/0009-2541\(86\)90004-5](https://doi.org/10.1016/0009-2541(86)90004-5)
- Munhtsengel, B., Chimedtseren, A., Javkhlan, O., Batkhishig, B., Altanzul, B., Soyolmaa, B., Burenjargal, O., Undarmaa, B., Ariuntsetseg, G., Manzshir, B., Munkh, J., Gerel, O., Tumurtogoo, O. 2018. Geology, magmatism, and mineralization of the paleo-subduction zones. Report of the Mongolian Foundation for Science and Technology Project No.ShUTT_012/2015, 450 p.
- Nasdala, L., Hofmeister, W., Norberg, N., Martinson, J. M., Corfu, F., Dörr, W., Kamo, S.L., Kennedy, A.K., Kronz, A., Reiners, P.W., Frei, D., Kosler J., Wan, Y., Götze J., Häger, T., Kröner, A., Valley, J.W. 2008. Zircon M257-a homogeneous natural reference material for the ion microprobe U-Pb analysis of zircon. *Geostandards and Geoanalytical Research*, v. 32(3), p. 247-265.
<https://doi.org/10.1111/j.1751-908X.2008.00914.x>
- Nguyen, H., Hanžl, P., Janoušek, V., Schulmann, K., Ulrich, M., Jiang, Y., Lexa, O., Altanbaatar, B., Deiller, P. 2018. Geochemistry and geochronology of Mississippian volcanic rocks from SW Mongolia: Implications for terrane subdivision and magmatic arc activity in the Trans-Altai Zone. *Journal of Asian Earth Sciences*, v. 164, p. 322-343.
<https://doi.org/10.1016/j.jseaes.2018.06.029>
- Pearce, J. 1996. Sources and settings of granitic rocks. *Episodes*, v. 19(4), p. 120-125.
<https://doi.org/10.18814/epiugs/1996/v19i4/005>
- Pearce, J.A. 2008. Geochemical fingerprinting of oceanic basalts with applications to ophiolite classification and the search for Archean oceanic crust. *Lithos*, v. 100(1-4), 14-48.
<https://doi.org/10.1016/j.lithos.2007.06.016>
- Pearce, J.A. 2014. Immobile Element Fingerprinting of Ophiolites. *Elements*, v. 10 (2), p. 101-108.
<https://doi.org/10.2113/gselements.10.2.101>
- Pearce, J.A., Cann, J.R. 1973. Tectonic setting of basic volcanic rocks determined using trace element analyses. *Earth and Planetary Science Letters*, v. 19(2), p. 290-300.

- [https://doi.org/10.1016/0012-821X\(73\)90129-5](https://doi.org/10.1016/0012-821X(73)90129-5)
 Pearce, J.A., Harris, N.B., Tindle, A.G. 1984. Trace Element Discrimination Diagrams for the Tectonic Interpretation of Granitic Rocks. *Journal of Petrology*, v. 25(4), p. 956-983. <https://doi.org/10.1093/petrology/25.4.956>
- Peccerillo, A., Taylor, S.R. Geochemistry of eocene calc-alkaline volcanic rocks from the Kastamonu area, Northern Turkey. *Contributions to Mineralogy and Petrology*, v. 58, p. 63-81. <https://doi.org/10.1007/BF00384745>
- Ruzhentsev, S. V., 2001, The Variscan Belt of South Mongolia and Dzungaria. In Dergunov, A.B., (Ed), *Tectonics, Magmatism, and Metallogeny of Mongolia*, London, Routledge, p. 61-94
- Ruzhentsev, S.V., Pospelov, I.I. 1992. The South Mongolia Variscan fold system: *Geotectonics*, v. 30, p. 383-395
- Safonova, I., Seltmann, R., Kroner, A., Gladkochub, D., Schulmann, K., Xiao, W., Kim, T., Komiya, T., Sun, M. 2011. A new concept of continental construction in the Central Asian Orogenic Belt (compared to actualistic examples from the Western Pacific). *Episodes*, v. 34(3), p. 186-196. <https://doi.org/10.18814/epiiugs/2011/v34i3/005>
- Schulmann, K., Paterson, S. 2011. Asian Continental Growth. *Nature Geoscience*, v. 4, p. 827-829. <https://doi.org/10.1038/ngeo1339>
- Sengör, A.C., Natal'in, B.A. 1996. Turkic-Type Orogeny and its Role in the Making of the Continental Crust. *Annual Review of Earth and Planetary Sciences*, v. 24(1), p. 263-337. <https://doi.org/10.1146/annurev.earth.24.1.263>
- Sláma, J., Košler, J., Condon, D.J., Crowley, J.L., Gerdes, A., Hanchar, J.M., Horstwood, M.S.A., Morris, G. A., Nasdala, L., Norberg, N., Schaltegger U., Schoene, B., Tubrett, M.N., Whitehouse, M.J. 2008. Plešovice zircon - A new natural reference material for U-Pb and Hf isotopic microanalysis. *Chemical Geology*, v. 249 (1-2), p. 1-35. <https://doi.org/10.1016/j.chemgeo.2007.11.005>
- Šourek, J., Černý, M., Reichert, M., 2003. Geological and Geochemical Mapping of Trans-Altay Gobi on the Scale 1:200 000. Unpublished manuscript, MRPAM, Ulaanbaatar.
- Sun, S.S., McDonough, W.F. 1989. Chemical and isotopic systematics of oceanic basalts: implications for mantle composition and processes. *Geological Society, London, Special Publications*, v. 42(1), p. 313-345. <https://doi.org/10.1144/GSL.SP.1989.042.01.19>
- Tasáryová, Z., Janoušek, V., Frýda, J. 2018. Failed Silurian continental rifting at the NW margin of Gondwana: evidence from basaltic volcanism of the Prague Basin (Teplá–Barrandian Unit, Bohemian Massif). *International Journal of Earth Sciences*, v. 107(4), p. 1231-1266. <https://doi.org/10.1007/s00531-017-1530-5>
- Tatsumi, Y. 2001. Geochemical modeling of partial melting of subducting sediments and subsequent melt-mantle interaction: Generation of high-Mg andesites in the Setouchi volcanic belt, southwest Japan. *Geology*, v. 29(4), p. 323-326. [https://doi.org/10.1130/0091-7613\(2001\)029<0323:GMOPMO>2.0.CO;2](https://doi.org/10.1130/0091-7613(2001)029<0323:GMOPMO>2.0.CO;2)
- Togtokh, J., Tumurchudur, Ch., Lkhundev, Sh., Oyunchimeg, T., Ganbayar, G., Khulan, B. 2020. Geodynamic problems, composition and ages of granitoid in the Edren Terrane. *Khaiguulchin*, v. 62, p. 26-39 (in Mongolian)
- Wang, X.C., Wilde, S.A., Xu, B., Pang, C.J. 2016. Origin of arc-like continental basalts: Implications for deep-Earth fluid cycling and tectonic discrimination. *Lithos*, v. 261, p. 5-45. <https://doi.org/10.1016/j.lithos.2015.12.014>
- Winchester, J.A., Floyd, P.A. 1977. Geochemical discrimination of different magma series and their differentiation products using immobile elements. *Chemical Geology*, v. 20, p. 325-343. [https://doi.org/10.1016/0009-2541\(77\)90057-2](https://doi.org/10.1016/0009-2541(77)90057-2)
- Windley, B. F., Alexeiev, D., Xiao, W., Kröner, A., Badarch, G. 2007. Tectonic models for accretion of the Central Asian Orogenic Belt. *Journal of the Geological Society*, v. 164(1), p. 31-47. <https://doi.org/10.1144/0016-76492006-022>
- Wood, D.A. 1980. The application of a Th-Hf-Ta diagram to problems of tectonomagmatic classification and to establishing the nature of crustal contamination of basaltic lavas of the British Tertiary Volcanic Province. *Earth and Planetary Science Letters*, v. 50(1), p. 11-30. [https://doi.org/10.1016/0012-821X\(80\)90116-8](https://doi.org/10.1016/0012-821X(80)90116-8)

- Xiao, W., Kusky, T. 2009, Geodynamic processes and metallogenesis of the Central Asian and related orogenic belts: Introduction. *Gondwana Research*, v. 16(2), p. 167-169.
<https://doi.org/10.1016/j.gr.2009.05.001>
- Xiao, W., Windley, B.F., Han, C., Liu, W., Wan, B., Zhang, J., Ao, S., Zhang, Z., Song, D. 2018. Late Paleozoic to early Triassic multiple roll-back and oroclinal bending of the Mongolia collage in Central Asia. *Earth-Science Reviews*, v. 186, p. 94-128.
<https://doi.org/10.1016/j.earscirev.2017.09.020>
- Xiao, W., Windley, B.F., Sun, S., Li, J., Huang, B., Han, C., Yuan, C., Sun, M., Chen, H. 2015. A tale of amalgamation of three collage systems in the Permian-Middle Triassic in Central Asia: Oroclines, sutures and terminal accretion. *Annual Review of Earth and Planetary Sciences*, v. 43, p. 477-507.
<https://doi.org/10.1146/annurev-earth-060614-105254>
- Yarmolyuk, V.V., Kovalenko, V.I., Sal’Nikova, E.B., Kovach, V.P., Kozlovsky, A.M., Kotov, A.B., Lebedev, V.I. 2008. Geochronology of igneous rocks and formation of the late Paleozoic south Mongolian active margin of the Siberian continent. *Stratigraphy and Geological Correlation*, v. 16(2), p. 162-181.
<https://doi.org/10.1134/S0869593808020056>
- Yuan, C., Sun, M., Xiao, W., Li, X., Chen, H., Lin, S., Xia, X., Long, X. 2007. Accretionary orogenesis of the Chinese Altai: Insights from Paleozoic granitoids. *Chemical Geology*, v. 242(1-2), p. 22-39.
<https://doi.org/10.1016/j.chemgeo.2007.02.013>
- Zhu, M., Zhang, F., Fan, J., Miao, L., Munkhtsengel, B., Anaad, C., Yang, S., Li, X., Ganbat, A. 2017. Late Carboniferous bimodal volcanic rocks and coeval A-type granite in the Suman Khad area, Southwest Mongolia: Implications for the tectonic evolution. *Journal of Asian Earth Sciences*, v. 144, p. 54-68.
<https://doi.org/10.1016/j.jseaes.2017.03.025>